EUR 397.e

REPRINT

ASSOCIATION EURATOM - C.E.A.
(European Atomic Energy Community - Commissariat à l'Energie Atomique)

SPECTROSCOPIC MEASUREMENTS ON A TITANIUM PLASMA GUN WITH HYDROGENATED ELECTRODES

by

H. W. DRAWIN
(Euratom)

1963

Work performed under the Euratom contract No. 007-62-1 FUAF

Reprinted from
ZEITSCHRIFT FÜR PHYSIK
Vol. 172, No. 2 - 1963

Zeitschrift für Physik 172, 181—201 (1963)

Groupe de Recherche de l'Association EURATOM-CEA sur la FUSION
Fontenay-aux-Roses (Seine); France

Spectroscopic Measurements on a Titanium Plasma Gun with hydrogenated Electrodes*

By
H.-W. DRAWIN

With 13 Figures in the Text

(Received August 13, 1962)

The plasma produced by a plasma gun which consists of concentric titanium and tantalum washers has been observed in the plasma gun as well as in a drift tube in which the plasma particles have been injected. Axial drift velocities of hydrogen and impurities have been determined in the drift tube by optical time-of-flight measurements. Maximum hydrogen velocities between $9 \cdot 10^6$ to $1 \cdot 10^8$ cm/sec could be determined, in agreement with magnetic probe-, Faraday cup-, microwave-, and electrostatic energy analyser measurements.
The plasma which is produced within the plasma gun by a powerful discharge (vacuum arc) has been observed with a framing camera, spectrographs and photomultipliers. From end-on observed time resolved spectrograms the temperatures and electron densities have been determined as a function of time. The measurements indicate that thermal equilibrium is reached about 2·5 μsec after the firing of the main discharge. 4 μsec after the beginning of the main discharge a maximum temperature of about 72000° K is reached. The measurements further indicate that the high-energy part of the ejected particles is produced before an equilibrium state in the plasma gun has been established.

§ 1. Introduction

This paper summarizes the results of spectroscopic measurements performed as a part of a study on the emission mechanism and the plasma properties of a titanium plasma gun used in the adiabatic magnetic compression experiment (Dispositif d'Etude de Compression Adiabatique = DECA). Measurements on this topic have been made sometimes ago by microwave, mass spectrometric, magnetic and electric probe techniques[1–10], but up to this date no spectroscopic data are

* Abbreviated publication of the report EUR-CEA-FC-170, Fontenay-aux-Roses, July 1962.

[1] FINKELSTEIN, D., G.A. SAYER and T.F. STRATTON: Phys. Fluids **1**, 188 (1958).

[2] EHLERS, K.W., J.D. GOW, L. RUBY and J. WILCOX: Rev. Sci. Instrum. **29**, 614 (1958).

[3] COENSGEN, F.H., W.F. CUMMINGS and A.E. SHERMAN: Phys. Fluids **2**, 350 (1958).

[4] COENSGEN, F.H., W.F. CUMMINGS and A.E. SHERMAN: Engineering Note UCRL-5603-T- 28. 5. 1959.

available. These spectroscopic measurements enable the plasma observation without perturbation of the plasma region by probe insertion, holes etc. ... The nature of the gas can be more easily and more accurately detected by spectroscopic techniques, thus giving some interesting additional information to the above mentioned probe measurements.

The measurements referred are devided in two different parts:

1. Observation of the plasma in the drift tube, with and without guiding magnetic field.

2. Observation of the plasma in the plasma gun proper.

Between these two parts there is a large difference in light emission due to the fast expanding low density plasma in the drift tube on the one hand and the high density plasma in the plasma gun on the other hand. Both parts demand their proper methods. At present the light emission from the drift tube is too weak to measure the whole plasma properties in this region, but nevertheless, the axial drift velocities of hydrogen and impurities were determined by a time-of-flight technique using spectroscopic means and photomultiplier detectors, and the trapping properties of the guiding magnetic field can be obtained.

On the contrary light emission of the plasma column within the plasma gun is rather luminuous, so that well exposed time resolved spectra can be obtained. Thus it is possible to calculate the plasma properties as a function of time without difficulties.

§ 2. Experimental Apparatus

For the purpose of our special investigation some details are of importance and will be described herafter.

2.1. Plasma gun and operating circuit

The plasma gun used in this experiment is made up of two concentric hydrogenated washers of titanium followed by twenty-one washers of tantalum, all of 12 mm internal diameter, 20 mm external diameter, and of 1 mm thickness. This type of gun was first described by EHLERS et al.[2],

[5] LECOUSTEY, P., C. RENAUD and J. TACHON: Rapport EUR-CEA-FC-128 (Fontenay-aux-Roses), Oct. 1961.

[6] BARIAUD, A., M. KORMAN, P. LECOUSTEY, J. LELEGARD, H. LUC and J. TACHON: Rapport EUR-CEA-FC-130 (Fontenay-aux-Roses), 1961, to be published in J. Nucl. Energy, part C (1962).

[7] LELEGARD, J., and H. LUC: Rapport EUR-SEA-FC-133 (Fontenay-aux-Roses), Dec. 1961.

[8] LUC, H.: Rapport EUR-CEA-FC-135 (Fontenay-aux-Roses), Dec. 1961.

[9] FAUGERAS, P.: Rapport EUR-CEA-FC-137 (Fontenay-aux-Roses), Dec. 1961.

[10] RENAUD, C., and J. TACHON: Rapport EUR-CEA-FC-162 (Fontenay-aux-Roses), May 1962.

and has further been developped by LELEGARD and LUC[7]. The special model used in this experiment is shown in Fig. 1: The first two Ti-washers are loaded with about 50% hydrogen. They are in electrical contact with a stainless steel end-electrode. The whole plasma gun is filled with 21 Ta-washers insolated from each other by ceramic rings. At the bottom a molybdenum trigger electrode is inserted. The plasma gun is flanged on a drift tube of pyrex glass of 15 cm internal diameter and 200 cm length. The pressure in the whole system is between $4 \cdot 10^{-7}$ and $2 \cdot 10^{-6}$ mm Hg during the measurements.

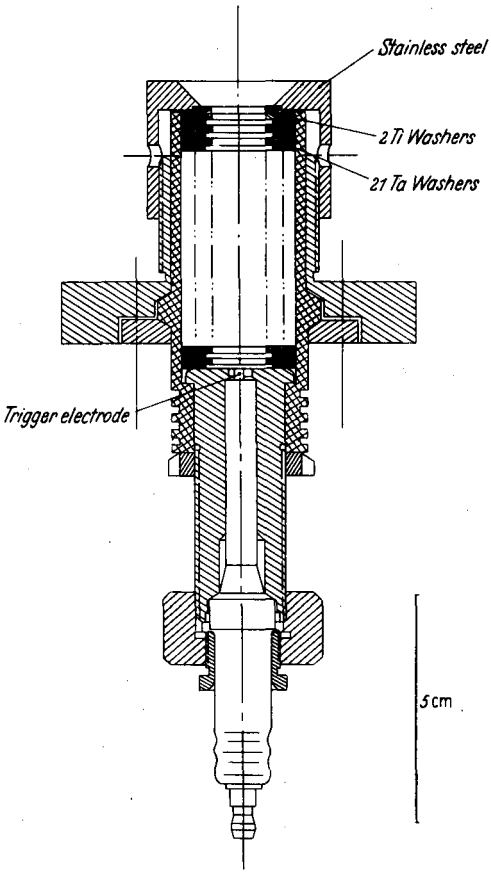

Fig. 1. Plasma gun

The operating circuit of the gun is shown schematically in Fig. 2: At time t_0 an initiating pulse is fed to a trigger pulser T_0 and a delay circuit R_1 which is followed by a second delay circuit R_2. At time t_0 a trigger pulse of about 30 kV is fired between the trigger electrode and the titanium washers, thus producing some charged particles which travel along the plasma gun. After a delay time $\Delta t_1 (\Delta t_1 \approx 1 \ldots 3\ \mu\text{sec})$ the main condenser ($C = 7{\cdot}73\ \mu\text{F}$; $U = 0 \ldots 18$ kV) is discharged through the gun via ignitron J_1, and at time $t_0 + \Delta t_2$ the gun is "crow-bared". The current through the gun and the voltage drop between the first and last electrode of the gun are shown in Fig. 3 for an initial voltage of 10 kV. The initial rise-time of the main discharge is $dJ/dt = 1.45 \cdot 10^{10}$ A/sec. The current and the voltage show small fluctuations of very short duration Δt ($\Delta t < 2 \cdot 10^{-7}$ sec). These fluctuations are probably produced by inhomogeneous metallic evaporation of the Ti- and Ta-washers or by the well known current-voltage fluctuations of fast pinches. These fluctuations have not further been investigated. But we would mention the fact that

the measured current and the photomultiplier signals are very similar to those, which have been obtained by ZWICKER[11] for pinches of higher pressures and higher atomic masses. In these case the kink-instabilities

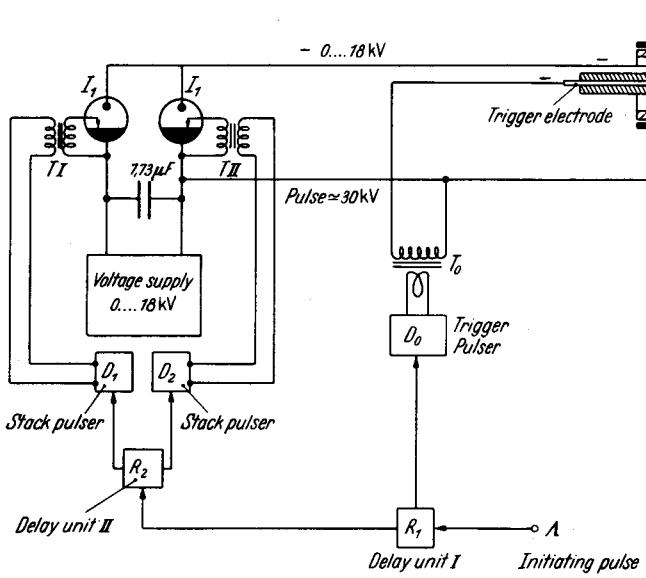

Fig. 2. Operating circuit for plasma gun

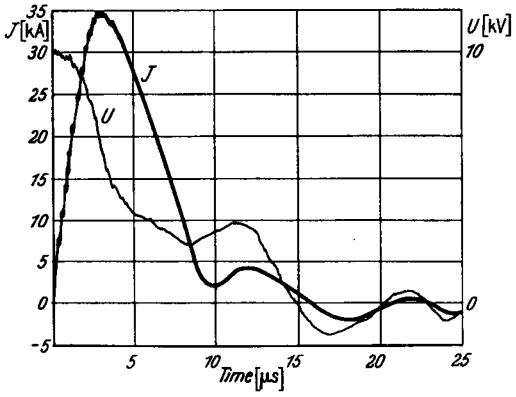

Fig. 3. Current J and voltage U of plasma gun

disappear, whereas small current fluctuations during the risetime of the current remain.

Als already mentioned before, the drift tube is surrounded by two coils for the production of an axial guiding magnetic field. Magnetic

[11] ZWICKER, H.: Proceedings of the 5th internat. Conf. on Ioniz. Phenomena in Gases, vol. II, p. 2175. Amsterdam: North-Holland Publ. Comp. 1962.

field strengths varied between $H=0$ Oe and $H=800$ Oe. Synchronisation between the firing of the plasma gun and the guiding magnetic field is shown in Fig. 4.

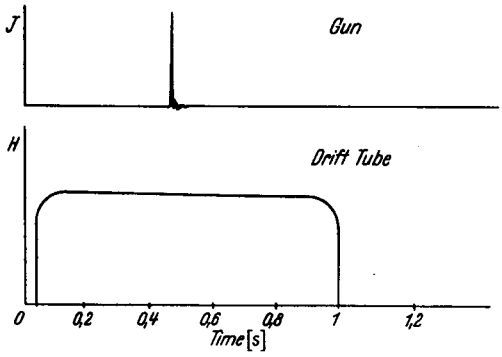

Fig. 4. Firing of plasma gun with respect to guiding magnetic field H

2.2. *Optical arrangement*

The position of the different spectrographs together with the drift tube and the reference standard light source is given in Fig. 5. Following McPherson[12] and Euler[13] a carbon arc was used as intensity standard

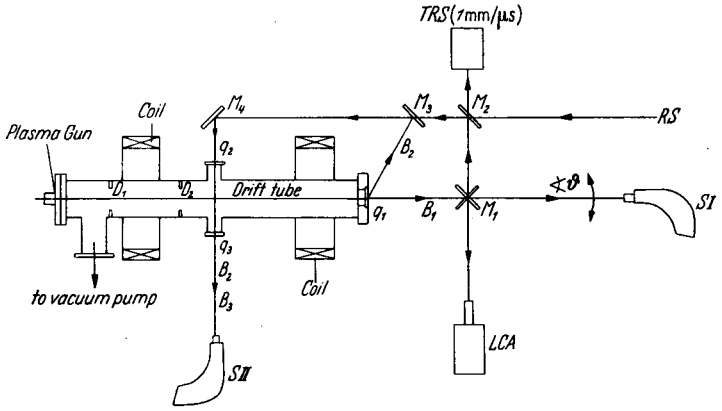

Fig. 5. Optical arrangement. *RS* standard light source, *S I*, *S II* spectrograph, *LCA* framing camera, *TRS* time resolving spectrograph

for relative and absolute calibration of the photographic plates, films and photomultipliers. An iron arc or low pressure discharge lamp served as wavelength calibration sources and as means to determine the instrumental broadening.

[12] McPherson, H. G.: J. Opt. Soc. Amer. **30**, 189 (1940).
[13] Euler, J.: Annal. Phys., VI. F. **11**, 203 (1953).

The following spectrographs and cameras have been used:

1. Hilger-Medium-Quartz-Spectrograph.

2. Huet-2 Prism-Glass-Spectrograph.

3. High-Speed Beaudouin-Camera with one glass prism as time resolving spectrograph (1.06 mm film/μsec).

4. L. C. A.-Framing-Camera, Type CI, with exposure time of 0.4 μsec per picture and a sequence of two pictures per μsec.

The first two spectrographs served either as time integrating instruments with photographic plates or as monochromators when photomultipliers were adapted. Observations have been made through three quartz-windows q_1-q_3; mirrors M_1-M_4 served for different light reflections. Further details are shown in Fig. 5.

2.3. Measurements

The light emitted from the plasmoids in the drift tube has been observed by light beams B_1, B_2 and B_3 respectively in side-on as well as in end-on observation for different spectral lines. To avoid the strong direct light from the plasma gun during the end-on observation of the plasma in the drift tube with spectrograph S_I (see Fig. 5), the latter has been taken a certain angle ϑ out of axis. Beams B_2 and B_3 served for side-on observation at two different points of the drift tube. To avoid further the detection of light signals from the plasma part in the wall region of the drift tube or from plasmoids, which have been reflected by the tube walls, two metallic screens D_1, D_2 have been inserted into the drift tube.

From the plasma gun end-on observed time-integrated and time-resolved spectra were obtained. The light emission from the plasma column of the gun is so strong, that well exposed pictures with a framing camera (aperture f/26) were possible. For the framing Camera Agfa-Rekord-films have been used.

The time-integrated spectra with spectrograph S_I or S_{II} have been made on low-speed Kodak-Plates II-L or II-F respectively. With an aperture of 1:12·5 only one shot was necessary to have a sufficiently strong exposition for the continuum.

For the time resolved spectra we have used Kodak-Royl-X-Pan-films. Photometric calibration has been made in each case with the carbon arc. To get a sufficiently high density from the carbon arc on the films, 10—12 mirror revolutions with an entrance slit width of $\frac{1}{5}$ ... 1 mm were necessary, whereas the spectra of the gun have been taken throughout with an entrance slit width of $\frac{1}{50}$ or $\frac{2}{50}$ mm respectively. The time resolution on the film was in both cases 1.06 mm/μsec.

To get the exact time relation between the current and the beam position on the film, light and current have been measured simultaneously with an oscilloscope. By comparing the oscilloscopic traces of the photomultiplier signal with the measured film intensities the starting point of the time scale on the film could be determined.

§ 3. Theoretical

In the described experiments light is observed from two different plasmas, namely one of high axial velocity but rather low density in the drift tube, and another of high density with strong light emission in the plasma gun. This fact involves two different types of formulas for the evaluation of the plasma properties, correlated respectively with the state of thermodynamic or non-thermodynamic equilibrium. Further, especially for the velocity determination one must be sure that the composition of the transient plasma in the drift tube does not change too much during the observation time. In other words, that the recombination time is sufficiently long compared with the observation time.

3.1. Plasma without thermodynamic equilibrium

3.1.1. Degree of ionization, rate of recombination, and velocity determination. The spectroscopical time-of-flight measurements require the following conditions:

1. The electron temperature T_e must be high enough to ensure a maximum degree of excitation (which is unfortunately related with a high degree of ionization).

2. The electron temperature T_e must be sufficiently low to give rise to a sufficiently high recombination rate for the different ions, especially hydrogen.

3. The relaxation time for recombination must be long enough compared with the measuring time.

These conditions are only fulfilled for certain temperatures and electron densities. Assuming equilibrium between ionization and recombination, the number of ionized particles can be calculated from the ionization formula which is valid for the corona of the sun[14,15] (neglecting photoionization and three-body impact recombination)

$$\frac{n_{r+1}}{n_r} = \frac{S_i}{Q_R} \tag{1}$$

[14] ELWERT, G.: Z. Naturforsch. **7**a, 432 (1952).
[15] KNORR, G.: Z. Naturforsch. **13**a, 942 (1958).

where r, $r+1$ indicate the ionization stages, and S_i, Q_R are the total ionization or recombination cross sections respectively. The ratio $\frac{n_{r+1}}{n_r}$ is independant of the electron density n_e and is given by (see [14])

$$\frac{n_{r+1}}{n_r} = 8.3 \cdot 10^5 \cdot \frac{f_2}{f_1} \cdot \frac{\xi_n}{g \cdot n} \left(\frac{E_i^H}{E_{in}}\right)^2 \frac{e^{-\frac{E_{in}}{kT_e}}}{\frac{E_{in}}{kT_e}} \tag{2}$$

if one assumes a Maxwellian-velocity-distribution of the electrons. It is

$f_1, f_2 \simeq 1$ (correction factors)

E_i^H = ionization energy of H

E_{in} = ionization energy for ionization process $n_r \rightarrow n_{r+1}$

ξ_n = number of bounded electrons in the n^{th}-shell.

Especially for the observation of hydrogen lines it is necessary to have a certain minimum number of neutral but excited particles. If the total particle density of hydrogen is of the order of 10^{15} cm^{-3}, the density of the neutrals should not be lower than 10^{13} cm^{-3}. With this maximum value $n_1/n_0 \simeq 10^2$ one calculates from equation (2) a maximum Maxwellian electron temperature of $T_e \simeq 2{\cdot}5 \cdot 10^4$ °K.

One can assume that the electron temperatures are much higher and therefore the observation conditions for hydrogen are much worse, because hydrogen is completely ionized and therefore not observable. The conditions for the observation of hydrogen lines would be better if the electrons were not thermalised, in other words: when the "high energy tail" — which is a consequence of the thermalisation process — has not yet been established. In this case the velocity distribution of the electron can be approximated by a Druyvesteyn-distribution. This distribution leads to much higher temperatures for the same ratio of the $r+1$- and r-fold ionized particles, a fact which has been pointed out very recently for instance by DEWAN[16].

The relaxation time τ_R for radiative recombination can be calculated from the total recombination coefficient Q_R. If

$$\frac{dn_{r+1}}{dt} = -Q_R n_e n_{r+1} \tag{3}$$

is the total disappearance of ions of type n_{r+1} by radiative capture, the relaxation time τ_R is of the order of

$$\tau_R \simeq \frac{1}{n_e Q_R}. \tag{4}$$

[16] DEWAN, E.M.: Phys. Fluids **4**, 759 (1961) and Report AFCRL 42 of U.S. Air Force Cambridge Research Laboratories, Bedford.

Assuming for the random velocities a Maxwellian electron velocity distribution, the total recombination coefficient is given by (see [17])

$$Q_R = 2ZA_R\left(\frac{2kT_e}{\pi m_0}\right)^{\frac{1}{2}}\beta\Phi(\beta) = 2.07\cdot 10^{-11}Z^3T_e^{-\frac{1}{2}}g\,\Phi(\beta), \tag{5}$$

where

$$\beta = \frac{h\nu_0}{kT_e} = \frac{1.57\cdot 10^5 Z^2}{T_e},$$

$$\Phi(\beta) = \sum_{n=1}^{n=n_{\max}\simeq\infty}\frac{\beta}{n^3}e^{\beta/n^2}\left\{-Ei\left(-\frac{\beta}{n^2}\right)\right\},$$

g = Gaunt factor (≈ 1).

With $Z = Z_{\text{eff}} = (Z+S)$ = effective nuclear charge

S = shielding factor ($\simeq 0 \ldots 0.5$)

an approximate calculation of recombination cross sections for not-hydrogen-like ions is also possible. For initial electron temperatures T_e of about 10^4 to 10^5 °K the relaxation times τ_R lie between 10^2 and $10^5\,\mu$sec, if the electron density is of the order of $n_e \simeq 10^{14}$ to 10^{15} cm^{-3}. The observation times are 10^1 to 10^2 times shorter than the above relaxation times. Therefore the measurements should not be affected by the radiative recombination coefficients of the different charged particles. The deexcitation time τ_D, which follows the recombination, has no further influence on the measurements, because

$$\tau_D \simeq \frac{1}{A_{mn}} \simeq 10^{-7}\,\text{sec} \ll \tau_R.$$

Thus, from the appearance of the different line signals the plasmoid velocity can directly be calculated from $v_Z = \frac{\Delta Z}{\Delta t}$.

3.2. Plasma in thermodynamic equilibrium

The main conditions for the establishment of a (local) thermodynamic equilibrium have been determined first by ORNSTEIN and BRINKMANN[18], and are:

$$\left.\begin{aligned}\Delta E = \Delta F \ll \tfrac{3}{2}kT.\\ \lambda\ \text{grad}\ T \ll T\end{aligned}\right\} \tag{6}$$

where Δ = electron (ion) mean free path

F = mean electric field strength

λ = thermal conductivity

T = temperature

ΔE = energy increase of a particle between two impacts.

[17] SPITZER, L.: Phys. of fully ionized Gases. New York: Interscience Publ. Inc. 1956.

[18] ORNSTEIN, L. S., and H. BRINKMANN: Physica, Haag **1**, 797 (1934).

These conditions are usually fulfilled in laboratory plasmas with densities higher than $\simeq 10^{16}\,\mathrm{cm}^{-3}$. For transient plasmas, a thermodynamic equilibrium is reached even if the time variations of the plasma parameters (temperature, densities) are much slower than the excitation-, ionization-, recombination- and deexcitation processes. This is the case up to times of $\simeq 10^{-7}$ sec. From the spectral line broadening we have found particle densities higher than $2.6 \cdot 10^{16}\,\mathrm{cm}^{-3}$.

This allows us to apply the Boltzmann-distribution for the excitation processes and especially the Saha-Eggert-equation for the calculation of the ratio of the charged particles.

The absolute line intensity J_{nm} of a spectral line per n_m excited particle per cm^{-3}, per sec and per unit solid angle is given by

$$J_{nm} = \int_{-\infty}^{+\infty} I(\lambda)\, d\lambda = \frac{1}{4\pi} A_{nm}\, n_m h\nu_{nm} \tag{7}$$

if observation bears on optical thin layers. With the Boltzmann distribution the number of particles n_m in the excited state m is

$$n_m = n \frac{g_m}{u(T)}\, e^{-\frac{E_m}{kT}} \tag{8}$$

and further the line intensity equal to

$$J_{nm} = \frac{1}{4\pi} \cdot \frac{g_m}{u(T)} A_{nm}\, n h\nu_{nm}\, e^{-\frac{E_m}{kT}}. \tag{9}$$

With A_{nm} = spontaneous transition probability for deexcitation
n = total particle density
g_m = statistical weight of state m
$u(T)$ = partition function
$h\nu_{nm} = E_m - E_n$.

With known particle densities the electron density can be calculated from the Saha-Eggert-equation $S_r(T)$ (see for instance[19])

$$S_r(T) = \frac{n_{r+1} \cdot n_e}{n_r} = \frac{2u_{r+1}(T)}{u_r(T)} \cdot \frac{(2\pi m_0 kT)^{\frac{3}{2}}}{h^3}\, e^{-\frac{E_r - \Delta E_r}{kT}}. \tag{10}$$

$u_{r+1}(T)$ and $u_r(T)$ are the partition functions of the $r+1$- and r-fold ionized atoms:

$$u_r(T) = \sum_0^\infty g_{r,s}\, e^{-\frac{E_{r,s}}{kT}} = g_0 + g_1 e^{-\frac{E_{r,1}}{kT}} + \cdots.$$

[19] UNSÖLD, A.: Physik der Sternatmosphären, 2. Aufl. Berlin-Göttingen-Heidelberg: Springer 1955.

ΔE_r is a small correction of the ionization energy E_r due to electric microfields, and is approximately given by

$$\Delta E_r \cong 7{\cdot}0 \cdot 10^{-7} Z^3 n_e^{\frac{1}{3}} [\mathrm{eV}]. \tag{11}$$

Equation (9) and (10) hold for each kind of particle. If the plasma consists of atoms and ions of different ionization degrees one has consequently a coupled system of equations from which the single particle densities and the temperature can be calculated. This method has been applied here by measuring the line intensities as a function of time, and solving then the corresponding system of equation.

3.3. Line broadening

The main broadening is due to the Doppler and Stark effects. Because of the high electron densities, the main broadening effect in the plasma gun is due to Stark effect. For the determination of electron densities from the H_α line* the Holtsmark-Profile with the correction given by GRIEM, KOLB and SHEN[20] has been used. Unfortunately, the Balmer lines are only emitted during a very short time at relatively low temperatures, whereas in our experiments rather high temperatures have been observed during a relatively "long time". Thus, the hydrogen atoms are completely ionized and the Balmer lines are no longer observable.

However, at higher temperatures, the elctron densities can be estimated using the distribution function $J_{nm}(\omega)$ of a spectral line as given by the classical impact theory (H. A. LORENTZ, V. WEISSKOPF, E. LINDHOLM, B. BURKHARDT et al.[19, 21])

$$J_{nm}(\omega) = \frac{\alpha}{\pi} \cdot \frac{1}{(\omega - \omega_0 + \beta)^2 + \alpha^2}. \tag{12}$$

For lines with quadratic Stark effect the theory leads to the following relations:

$$\textit{shift}: \quad (\omega - \omega_{\max})_4 = \beta_4 = 9.85 \cdot C_4^{2/3} v_{\mathrm{rel}}^{1/3} n_e$$
$$\textit{full half width}: \quad \gamma_4 = 2\alpha_4 = 11.37 \cdot C_4^{2/3} v_{\mathrm{rel}}^{1/3} n_e.$$

For shift $\Delta\lambda_S$ and full half width $2\Delta\lambda_H$ in Angström units [Å] one has

$$\Delta\lambda_S = 1.57 \cdot 10^{-8} \frac{\lambda^2}{c} C_4^{2/3} \cdot v_{\mathrm{rel}}^{1/3} \cdot n_e,$$

$$2\Delta\lambda_H = 1.81 \cdot 10^{-8} \frac{\lambda^2}{c} C_4^{2/3} v_{\mathrm{rel}}^{1/3} n_e.$$

* The $H\beta$-line is disturbed by many impurity lines of Oxygen and Carbon.

[20] GRIEM, H.R., A.C. KOLB and K.Y. SHEN: Phys. Rev. **116**, 4 (1959 and NRL-Report No. 5455 (1960).

[21] TRAVING, G.: Über die Theorie der Druckverbreiterung von Spektrallinien, Karlsruhe: G. Braun 1960.

C_4 is the Stark effect constant which corresponds to the frequency shift

$$\Delta\omega_4 = \frac{2\pi C_4}{r^4}.$$

v_{rel} is the average velocity of electrons in the case of quadratic Stark effect. With known C_4-values the densities of the electrons can be determined. Unfortunately C_4-values are unknown for nearly all ionic lines, excepted He. Nevertheless one can insert C_4-values of the approximate order of magnitude which gives then an approximate order of magnitude for the electron densities. By this method one can at least verify if the assumption of a (local) thermodynamic equilibrium was correct. For the approximate determination of n_e the exact value of v_{rel} is not necessary. If one takes only an estimated value for the temperature T, v_{rel} is sufficiently well determined due to the relation

$$v_{\mathrm{rel}}^{1/3} \sim T^{1/6}.$$

The C_4-values for He I- and He II-lines are of the order of 10^{-12} to 10^{-13} el. st. units, for A, Ne, Kr of the order of 10^{-13} to 10^{-16} el. st. units[19, 21, 22].

3.4. Correction for instrumental broadening

The measured line profiles have been corrected for instrumental broadening so far as necessary. The iterative method of BURGER and VAN CITTERT[19, 23, 24] was used in the following way:

If $f(\Delta\lambda)$ is the true profile of a spectral line, $g(\Delta\lambda)$ is the profile recorded by the spectrograph and $k(\Delta\lambda)$ is the apparatus function, one has the relation

$$g(\Delta\lambda) = \int_{-\infty}^{\infty} f(\Delta\Lambda)\, k(\Delta\lambda)\, d(\Delta\Lambda).$$

It is now possible to use $g(\Delta\lambda)$ as a first approximation, $f_0(\Delta\lambda)$, to $f(\Delta\lambda)$. Better approximations are calculated successively from

$$g_i(\Delta\lambda) = \int f_i(\Delta\Lambda)\, k(\Delta\lambda - \Delta\Lambda)\, d(\Delta\Lambda)$$
$$f_{i+1}(\Delta\lambda) = f_i(\Delta\lambda) + g(\Delta\lambda) - g_i(\Delta\lambda)$$

When $g(\Delta\lambda) - g_i(\Delta\lambda)$ and $f_{i+1}(\Delta\lambda) - f_i(\Delta\lambda)$ are sufficiently small the iteration is terminated. Convergence can be quite rapid. We have finished the calculations after the second step.

---

[22] LANDOLT-BÖRNSTEIN: Zahlenwerte und Funktionen, 6. Aufl., Bd. 1, Teil 1. Berlin-Göttingen-Heidelberg: Springer 1950.

[23] BURGER, H.C., u. P.H. VAN CITTERT: Z. Physik **79**, 722 (1932); **81**, 428 (1933).

[24] ROLLET, J.S., and L.A. HIGGS: Proc. Phys. Soc. Lond. **79**, 87 (1962).

§4. Results

4.1. Drift tube

4.1.1. Axial particle velocities. The line intensities of different spectral lines have been measured by observing light beams B_2 and B_3 (Fig. 5) from two different points with a photomultiplier adapted to the spectrograph S_{II}. From the observation times the velocities have been calculated as has been outlined above.

Typical oscillograms for some lines are given in Fig. 6—9 corresponding to a condenser voltage of $U=10$ kV. The following facts are remarkable: The different elements show different characteristic variations with time of the light signals. Each element has a certain "characteristic intensity profile". These profiles are not completely reproducible from one discharge to another, but show fluctuations of the absolute amount of the light signals. Maximum variations from one shot to another can be $\pm 50\%$. Also the appearance of the maximum can change with time, normally the variations are ± 25 to $\pm 30\%$. Further the fine fluctuations of the signal change somewhat for different discharges. But the typical profile of the signal for the different elements remains roughly the same.

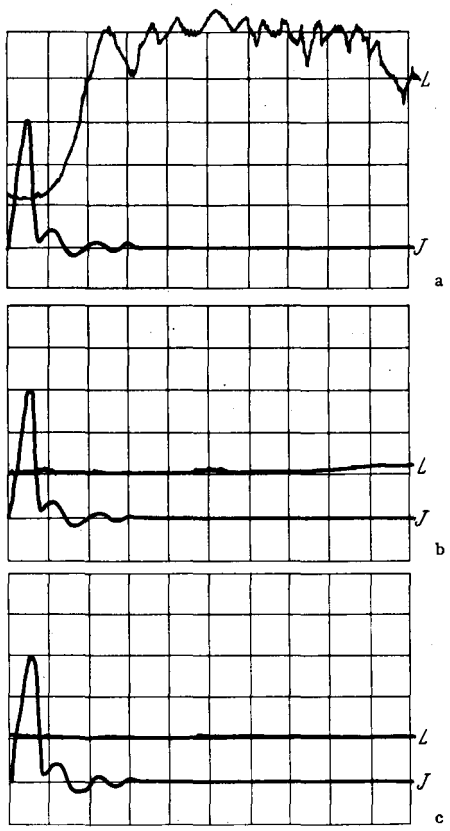

Fig. 6a—c. Observation of $H\beta$-line through window $q3$; time base 10 μsec/cm. a $H=800$ Oe; b $H=0$ Oe; c spectrograph closed

From the oscillograms we have calculated the maximum, the average and the minimum velocities. The maximum velocity v_{max} is the highest velocity, calculated from the first moment of observation of a certain spectral line. The average velocity v_{aver} is that velocity which is correlated with the maximum light signal (= gravity center). The minimum velocity is correlated to that intensity signal where the line intensity has fallen to $\simeq 30\%$ of the maximum value at the gravity center. The obtained values are given in Table 1, with an accuracy of about ± 25 to

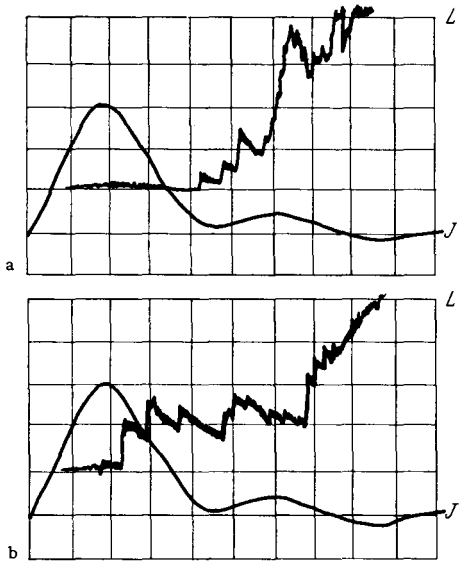

Fig. 7 a u. b. Observation of $H\beta$ (λ 4861 Å) through window $q3$. Normally Fig. 8a, but sometimes high velocities according to Fig. 8b are observed; time base 2 μsec/cm; L light; J current

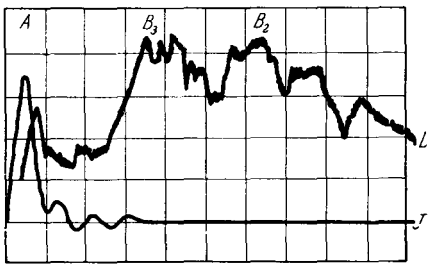

Fig. 8. Observation of C III-line λ 4650 Å through windows $q1$ and $q3$ at the same time (first weak maximum A at $t = 7$ μs originates from direct light of the plasma gun, peak B_2, B_3 correspond to lightbeams B_2. B_3 respectively. Time base 10 μsec/cm; L light; J current

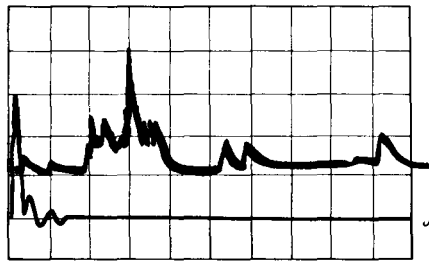

Fig. 9. Observation of Al I line λ 3961 Å through window $q3$. Time base 20 μsec/cm. L light; J current

30%, except for hydrogen. The origin of time of the emission is calculated to be between 0 and $2\frac{1}{2}$ μsec after the beginning of the main discharge. After $2\frac{1}{2}$ μsec the emission is negligable small.

Some particularities should be mentioned: Normally for hydrogen (measured on the $H\beta$ line λ 4861 Å) the line intensity rises rather sharply at a well defined point. The corresponding velocities range from about $9 \cdot 10^6$ to $4 \cdot 10^7$ cm/sec. Sometimes however the hydrogen signals occur much earlier, thus indicating a higher velocity up to $1 \cdot 10^8$ cm/sec, corresponding to an axial energy of 5.5 keV. This typical phenomenon is shown in Fig. 7a and 7b.

The longest signals have been observed for the hydrogen emission. The intensity curves are rather flat. Two reasons may be responsible for this phenomenon:

1. A rather long recombination time τ_R.

2. The walls of the pyrex tube are contaminated with hydrocarbons from the oil diffusion pump. The plasma touches the walls after a certain time with rather high energies, and liberates and excites mainly hydrogen which then gives an additional emission.

On the contrary, carbon and mainly alluminium show rather sharp intensity peaks.

Measurements with different guiding fields between $H = 150$ and

800 Oe. showed only a small increase of v with H. This increase is not very significant and the results obtained are in agreement with the measurements of BARIAUD et al.[6] and RENAUD and TACHON[10] with about the same incertities.

Table 1. *Axial velocities v [cm/sec] for U=10 kV and a guiding field of H=800 Oe (derived from line intensities)*

Element	v_{max}	v_{aver}	v_{min}
H	$0.9-4 \cdot 10^7$ ($1 \cdot 10^8$)	$2 \cdot 10^6$	$3 \cdot 10^5$
C	$0.7-1 \cdot 10^7$ ($2 \cdot 10^7$)	$2 \cdot 10^6$	$1 \cdot 10^6$
O	$8 \cdot 10^6$	$2 \cdot 10^6$	$1 \cdot 10^6$
Si	$8 \cdot 10^6$	$2 \cdot 10^6$	$1 \cdot 10^6$
Mg	$1 \cdot 10^7$	$2 \cdot 10^6$	$1 \cdot 10^6$
Al	$8 \cdot 10^6$	$1.6 \cdot 10^6$	$\simeq 7 \cdot 10^5$
Other elements	$\simeq 8 \cdot 10^6$	$2 \cdot 10^6$	$7 \cdot 10^4$

4.1.2. Particle confinement of guiding field. The particle confinement of the guiding magnetic field is shown in Fig. 6 for the field strength $H=0$ and $H=800$ Oe. The line intensity is negligibly small for zero guiding magnetic fields, whereas for increasing magnetic fields H the line intensities increase $\simeq$ proportional to H in the range $H=0$ and 800 Oe. In Fig. 6c an additional reference trace is given corresponding to the spectrograph with its slit closed, (but with a guiding field of $H=800$ Oe).

4.2. Plasma gun

Pictures have been taken with a L. C. A.-Framing Camera, type CI, for different condenser charging voltages. The pictures show that the beginning of the discharge is in nearly all cases asymmetric, probably due to the different velocities of evaporation of the metallic washers and the bottom electrode. The luminuous column is then built up in about 2 to $2\frac{1}{2}$ μsec. During the first half period of the current, the column remains stable whereas for the following half periods instabilities in the column position occur.

A time integrated spectrum is shown in Fig. 10. The very strong continuous emission over the whole wavelength range is quite remarkable and similar to what has been found in shock wave experiments and in large pinch discharges[11, 25]. This continuous emission exceeds in some cases even the intensities of the strongest impurity lines, so that the measurement of the line wings and the separation of the line wings from the background becomes rather difficult.

[25] BÖTTICHER, W.: Proceedings of the 5th Intern. Conf. on Ionization Phenomena in Gases, vol. II, p. 2183. Amsterdam: North-Holland Publ. Comp. 1962.

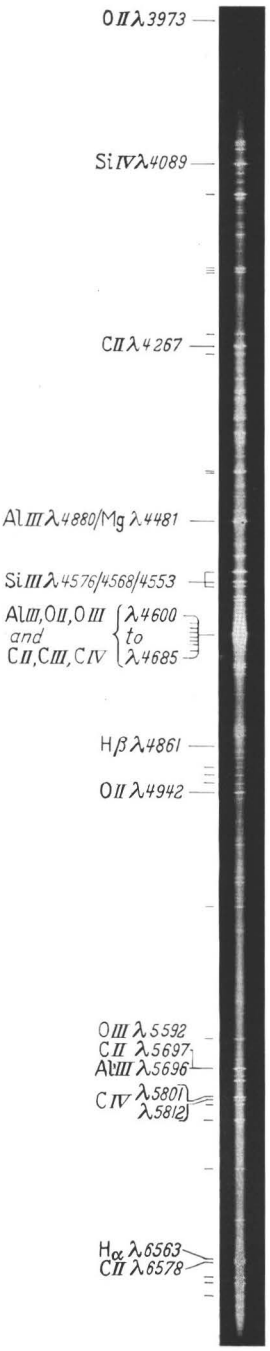

Fig. 10

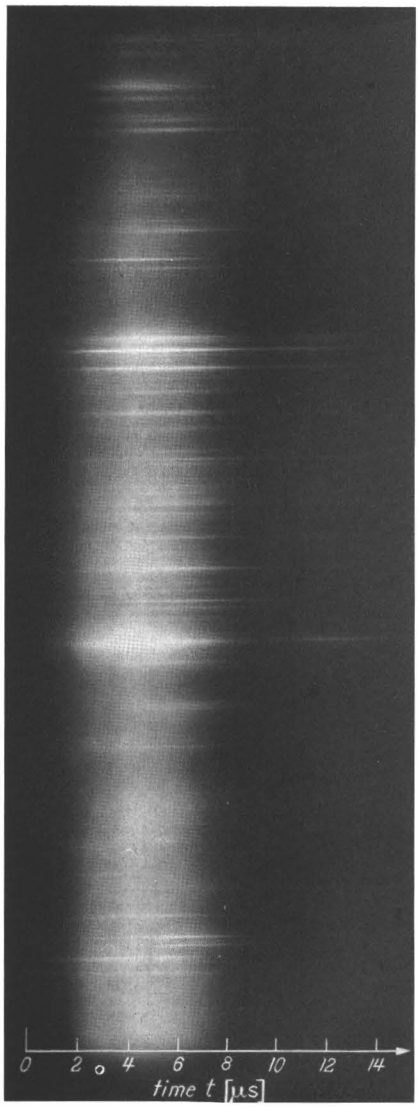

Fig. 11

Fig. 10. Time-integrated spectrum of plasma gun (1 shot on Kodak-Plate II-L)

Fig. 11. Time-resolved spectrum of plasma gun (1 shot on Kodak-film Royl-X-Pan). At time $t = 0$ beginning of the current through the gun. Spectral lines as in Fig. 10

Table 2. *Full half width $2\Delta\lambda_H$ from time integrated spectra*

Element	λ [Å]	Transition	E_m [eV]	$2\Delta\lambda_H$ [Å]
H	6562.8	$2^2P^0 - 3^2D$	12.04	5
	4861.3	$2^2P^0 - 4^2D$	12.69	≈ 30
C I	4826.7	$3s^3P_2^0 - 4^3p\,S_1$	10.01	3.5
C II	4267.02	$3^2D_{5/2} - 4^2F_{7/2}^0$	20.86	0.72
	4267.29	$3^2D_{3/2} - 4^2F_{5/2}^0$	20.86	
C III	2296.9	$2p^1P_1^0 - 2p^1D_2$	18.72	0.34
	4647.4	$3^3S_1 - 3^3P_2^0$	32.05	1.2
C IV	5801.5	$3^2S_{1/2} - 3^2P_{3/2}^0$	39.51	2.74
	5812.1	$3^2S_{1/2} - 3^2P_{1/2}$	39.51	2.86
O II	3973.3	$3s^2P_{3/2} - 3p^2P_{3/2}^0$	26.45	0.52
	4072.2	$3p^4D_{5/2}^0 - 3d^4F_{7/2}$	28.57	0.58
	4075.9	$3p^4D_{7/2}^1 - 3d^4F_{9/2}$	28.58	0.53
	4317.1	$3s^4P_{1/2} - 3p^4P_{3/2}^0$	25.73	0.80
	4319.6	$3s^4P_{3/2} - 3p^4P_{5/2}$	25.74	0.69
O III	3047.1	$3s^3P_2^0 - 3p^3P_2$	37.09	0.57
	3059.3	$3s^3P_2^0 - 3p^3P_1$	37.07	0.54
	3312.3	$3s^3P_2^0 - 3p^3S_1$	36.73	0.65
O IV	3063.5	$3^2S_{1/2} - 3^2P_{3/2}^0$	48.18	0.57
	3071.7	$3^2S_{1/2} - 3^2P_{1/2}^0$	48.17	0.52
O V	2781.0	$3s^3P_1^0 - 3p^3P_2$	85.6	0.66
	2787.1	$3s^3P_1^0 - 3p^3P_1$	85.7	0.70
Al III	4512.5	$4^2P_{1/2}^0 - 4^2D_{3/2}$	20.47	1.37
Si I	2519.1	$3p^3P_1 - 4s^3P_2^0$	4.93	0.76
Si II	4128.1	$3^2D_{3/2} - 4^2F_{5/2}$	12.78	0.54
	4130.9	$3^2D_{5/2} - 4^2F_{5/2}^0$	12.78	0.53
Si III	3096.8	$3^3D_1 - 4^3P_0^0$	21.62	0.84
	4552.7	$4^3S_1 - 4^3P_2^0$	21.63	0.85
	4567.9	$4^3S_1 - 4^3P_1^0$	21.62	0.85
	4574.8	$4^3S_1 - 4^3P_0^0$	21.62	0.86
Si IV	4088.9	$4^2S_{1/2} - 4^2P_{3/2}^0$	26.97	0.64
	4116.1	$4^2S_{1/2} - 4^2P_{1/2}^0$	26.95	0.59

The measured half width of the lines exceeds in all cases several times the Doppler broadening. The main broadening effect must therefore be due to the Stark effect broadening of the microfields.

Indeed, no relation could be found between the velocity distribution of the ejected plasma and the line emissions in the plasma gun.

The half widths of the strongest lines have been measured using the time integrated spectra. The results are summarized in Table 2. The actual line widths are probably several times larger, because

1. Time integration favours the intensity of the line center, considerable emission originating from lower plasma temperatures.

2. High microfield strenths favour the broadening of the line wings since for the tail components a change from quadratic to linear Stark effect begins much earlier than for the components near the center. Thus, the line wing extremities disappear in the continuous background. Both effects lead consequently to a smaller effective line width.

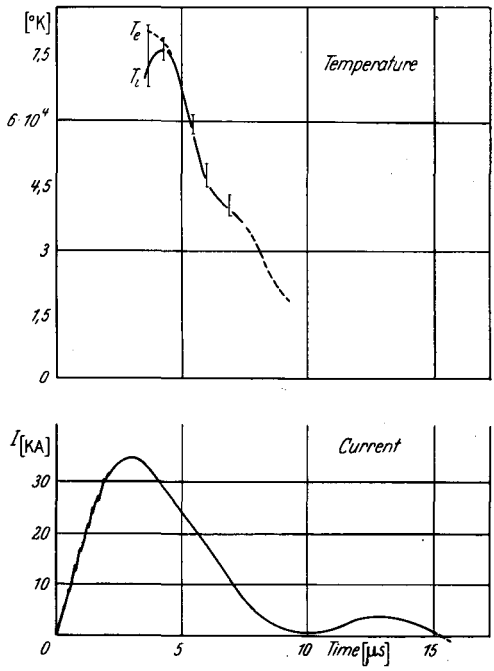

Fig. 12. Temperature T as function of time

From the comparison of the theoretical and measured line profile of $H\alpha$ (λ6563 Å) an ion density of $2.6 \cdot 10^{16}$ cm^{-3} is obtained as shown in Fig. 13. This "mean density" corresponds only to a relatively low temperature, since hydrogen being completely ionized for higher temperatures.

Application of the damping equation (12) to the line profiles of the highly ionized atoms enables to calculate — with a mean Stark effect constant $C_4 \cong 10^{-15}$ el. st. units for the C-, or O-Lines — a particle density of the order of $n_e \simeq 4 \cdot 10^{17}$ cm^{-3}. With these high densities, the formulas for thermodynamic equilibrium can be applied as outlined above.

An evaluation of the time resolved spectra leads to the following results: During the first two microseconds after the beginning of the current, the light-emission is rather weak and the plasma column is not well defined. But after two microseconds, just before the current reaches its maximum value, the emission of the continuous spectrum and of the highest ionic lines increases very rapidly. This maximum emission is followed by a slower decrease of several microseconds, during which the lower ionic lines appear. An application of the above mentioned method to

C-, O-, or Si-lines for the temperature and particle determination leads to a maximum temperature of at least $T = 72000°$ K. For this temperature an electron density of $n_e \simeq 6 \cdot 10^{18}$ cm^{-3} is reached. Temperature and electron density fall then rapidly down as shown in Fig. 12. From the measurements of the absolute intensities of the impurities C, Si, Mg, O, Al etc. a maximum particle density of 10^{15} to 10^{16} cm^{-3} was calculated. If one assumes a mean charge of $Z = 3$ to 4, the electron density should not be higher than $\simeq 8 \cdot 10^{16}$ cm^{-3}. The high densities up to $6 \cdot 10^{18}$ cm^{-3} must therefore be produced by a strong evaporation and ionization of the

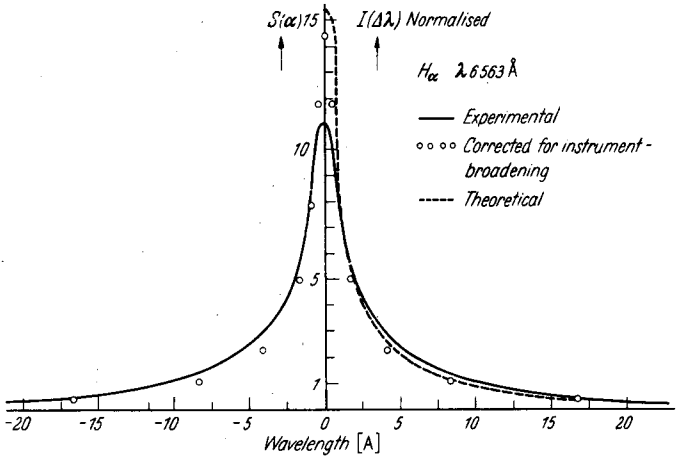

Fig. 13. Comparison of measured and calculated line profile of $H\alpha$ (Time integrated). $n_e = 2.6 \cdot 10^{16}$ cm^{-3}; $T = 20000°$ K

bottom electrode and of the tantalum-washers, the spectra of which have not been observed since their very weak line intensities disappear in the high continuous background. Unfortunately nothing can be said on the absolute intensities of the higher ionic lines of tantalum because the spectra are unknown until to date. Also the ionization energies are not known. But if we assume a mean charge of $Z = 6$ to 8 for the tantalum ions (due to the position in the periodic system the ionization energies should follow each other very closely), the tantalum density would be of the order of $7 \cdot 10^{17}$ to $1 \cdot 10^{18}$ cm^{-3}. This density can easily be obtained as a result of sputtering and evaporation of the washers.

The temperature determination used here is based on the assumption of a nearly homogeneous plasma column with the same temperature in all parts and without large self absorption. This assumption is justified by the fact that the spectral lines for the different ionization stages just follow the decrease of temperature on the one hand, and a decrease of the line intensity in the line center was not observable on the other hand.

If there exists an appreciable variation of temperature or density with the length of the plasma column the mean temperature would be somewhat lower as calculated here. But this can be verified only by side-on measurements at different points of the gun.

§ 5. Summary

From spectroscopic measurements described above the properties and mechanism of the plasma gun can now be understood as follows: During the firing of the trigger pulse at time t_0 and during the first 2 to $2\frac{1}{2}$ μsec of the main discharge through the gun hardly no light emission can be observed which is related with a quasi-stable state of the plasma column. The plasma density in the gun must be small and there is no thermodynamic equilibrium. Time-of-flight measurements indicate that the time-origin of the plasma emission lies between 0 and $2\frac{1}{2}$ microseconds after the beginning of the discharge. The maximum velocities for hydrogen range normally from 0.9 to $4 \cdot 10^7$ cm/sec, sometimes to $1 \cdot 10^8$ cm/sec, whereas the average velocity of the center of mass is about $2 \cdot 10^6$ cm/sec for nearly all ejected particles. It is not excluded that current and voltage fluctuations, which can be observed during the first current increase (0 ... 2 μsec), are related to the plasma ejection.

$2\frac{1}{2}$ μsec after the beginning of the main discharge a strong light emission is observed. Both time-integrated and time-resolved spectra lead to a high density and high temperature plasma in thermodynamic equilibrium (see Fig. 12). A maximum temperature of about 72000° K is reached 4 μsec after the firing of the discharge and 1 μsec after the current has passed its maximum value. The recombination of the plasma takes then place in about 3 to 4 μsec.

After the attainment of the thermodynamic equilibrium in the gun the latter is blocked for further ionic emission of the emission of particles of high axial energy.

The main current peak is followed by some smaller current oscillations. The light emission during these oscillations is negligibly small in comparison with the emission during the first half period.

Comparison with the measurements of BARIAUD et al.[6] and RENAUD and TACHON[10] indicates, mainly for hydrogen, the same axial velocities. But we should emphasize that in the case of velocity determinations by magnetic probe measurements the hydrogen velocities are related to peak signals, whereas in our measurements the high velocities are connected with the first appearance of the signal. A high velocity "hydrogen-peak" has not been observed probably due to the fact that nearly all hydrogen atoms were ionized.

A very striking fact is the same average axial velocity of $v_{aver} \approx 2 \cdot 10^6$ cm/sec for all impurities independent from the particle mass m (see Table 1). One should think, that the average energy E_{aver} of the gravity center would be a constant, thus leading to different velocities $v_{aver} = \sqrt{\frac{2E_{aver}}{m}}$ for the different atomic species. These different average velocities could not be observed. The reason for this fact is probably the following one: The line intensities are produced by excitation and recombination processes. Both effects are proportional to the electron density n_e. The electron density is thus able to change the product $n_{i-1}\, n_e$ or $n_i n_e$ respectively which give after all the line intensities. The same average velocity of $\simeq 2 \cdot 10^6$ cm/sec for all particles indicates that this velocity corresponds probably to a "plasmoid-buble" with a high electron density. This electron density favours the excitation and recombination for *all* particles in the same manner. Thus, due to these high values of n_e, the line intensities have a maximum for all particles at nearly the same time. The high-density "plasmoid-buble" with $v_{aver} \cong 2 \cdot 10^6$ cm/sec in the drift tube is probably tantalum.

At present the light emission from the drift tube is too weak to measure the whole plasma properties as a function of time and geometry by the conventional spectroscopic techniques. When the plasma density of the ejected plasmoids and thus the light emission could be increased by about a factor ten, a quantitative analysis should be possible, presumed that the atomic constants such as spontaneous transition probabilities, ionization- and recombination cross sections are available and the velocity distribution of the electrons is known.

Author would thank Mr. SABLON for helpful work during the experiments and for numerical calculations.